

This document is the unedited Author's version of a Submitted Work that was subsequently accepted for publication in the

ACS APPLIED MATERIALS & INTERFACES,
copyright © American Chemical Society after peer review.

To access the final edited and published work see

<https://pubs.acs.org/doi/abs/10.1021/acsami.8b18435>

DOI: [10.1021/acsami.8b18435](https://doi.org/10.1021/acsami.8b18435)

Reference: *ACS Appl. Mater. Interfaces* **2019**, *11*, 5947-5956

Integrating Water-Soluble Polythiophene With Transition Metal Dichalcogenides for Managing Photoinduced Processes

Ruben Canton-Vitoria,^{¶#} Emin Istif,^{§#} Javier Hernández-Ferrer,[§] Esteban Urriolabeitia,[‡] Ana M. Benito,^{§} Wolfgang K. Maser,^{*§} Nikos Tagmatarchis^{*¶}*

[¶] Theoretical and Physical Chemistry Institute, National Hellenic Research Foundation, 48 Vassileos Constantinou Avenue, 11635 Athens, Greece.

[§] Instituto de Carboquímica – CSIC, C/Miguel Luesma Castán 4, E-50018 Zaragoza, Spain.

[‡] Instituto de Síntesis Química y Catálisis Homogénea CSIC, Universidad de Zaragoza, C/Pedro Cerbuna 12, E-50009 Zaragoza, Spain.

[#]These authors have equally contributed.

Integrating Water-Soluble Polythiophene With Transition Metal Dichalcogenides for Managing Photoinduced Processes

*Ruben Canton-Vitoria,^{¶#} Emin Istif,^{§#} Javier Hernández-Ferrer,[§] Esteban Urriolabeitia,[‡] Ana M.
Benito,^{*§} Wolfgang K. Maser,^{*§} Nikos Tagmatarchis^{*¶}*

[¶]Theoretical and Physical Chemistry Institute, National Hellenic Research Foundation, 48
Vassileos Constantinou Avenue, 11635 Athens, Greece.

[§] Instituto de Carboquímica – CSIC, C/Miguel Luesma Castán 4, E-50018 Zaragoza, Spain.

[‡] Instituto de Síntesis Química y Catálisis Homogénea CSIC, Universidad de Zaragoza
C/Pedro Cerbuna 12, E-50009 Zaragoza, Spain.

[#]These authors have equally contributed.

KEYWORDS: transition metal dichalcogenides, polythiophenes, functionalization, electrostatic interactions, photophysics, photoelectrochemistry.

ABSTRACT

Transition metal dichalcogenides (TMDs) attract increased attention for the development of donor-acceptor materials enabling improved light harvesting and optoelectronic applications. The development of novel donor-acceptor nanoensembles consisting of poly(3-thiophene sodium acetate) and ammonium functionalized MoS₂ and WS₂ was accomplished, while photoelectrochemical cells were fabricated and examined. Attractive interactions between the negatively charged carboxylate anion on the polythiophene backbone and the positively charged ammonium moieties on the TMDs enabled in a controlled way and in aqueous dispersions the electrostatic association of two species, evidenced upon titration experiments. A progressive quenching of the characteristic fluorescence emission of the polythiophene derivative at 555 nm revealed photoinduced intra-ensemble energy and/or electron transfer from the polymer to the conduction band of the two TMDs. Photoelectrochemical assays further confirmed the establishment of photo-induced charge-transfer processes in thin films, with distinct responses for the MoS₂ and WS₂ based systems. The MoS₂-based ensemble exhibited enhanced photoanodic currents offering additional channels for hole-transfer to the solution, while the WS₂-based one displayed increased photocathodic currents providing supplementary pathways of electron-transfer to the solution. Moreover, scan-direction depending photoanodic and photocathodic currents suggested the existence of yet unexploited photoinduced memory effects. These findings highlight the value of electrostatic interactions for the creation of novel donor-acceptor TMD-based ensembles and their relevance for managing the performance of photoelectrochemical and optoelectronic processes.

INTRODUCTION

Transition metal dichalcogenides (TMDs), with most representative and studied members MoS₂ and WS₂, have attracted great consideration in the last few years as a result of their unique optical, electronic and catalytic properties.^{1, 2} Without surprise, MoS₂ and WS₂ have also been considered potentially suitable for diverse applications, spanning from energy conversion and storage (solar cells, batteries, supercapacitors)³⁻⁵ to sensing and photo- and electro-catalysis.^{6,7} However, in order to take full benefit of the novel characteristics of MoS₂ and WS₂, manipulation in wet media and hybridization with other functional materials is required. The latter can be realized by chemically functionalizing TMDs with organic materials, en route the development of ensembles with intriguing properties directly derived from the inherent characteristics of the two species. The integration of functional species on MoS₂ and WS₂ can be achieved either via covalent bonding or through supramolecular interactions.⁸ In addition, surface functionalization permits managing the charge carrier density, by inducing or removing defects, therefore allowing to tune and control the optoelectronic properties of TMDs,⁹ which are dominated by excitonic transitions.^{10, 11}

In recent years, the functionalization of exfoliated TMDs steadily expands and diverse strategies are nowadays available allowing their modification in a facile way. For example, aryl diazonium salts and organoiodides have been employed to decorate the basal plane of MoS₂ with organic addends,^{12, 13} while functionalization with thiols has been achieved, though without clear evidence if the thiol is bound or has been converted to the corresponding disulfide that is eventually physisorbed onto the MoS₂.¹⁴ However, a more straightforward route for obtaining functionalized MoS₂ and WS₂ involves reaction with 1,2-dithiolanes, which possess high binding affinity for Mo and W atoms with S vacant sites located at the edges.¹⁵ In fact, with the latter approach, innovative hybrid materials with interesting photophysical and/or electrocatalytic

properties were prepared, also with the advantage of preserving intact the basal plane since the functionalization reaction occurs only at edges, where the majority of S defects are concentrated. As prominent paradigms, incorporation of pyrene and carbon nanodots (CNDs) on MoS₂,^{15, 16} and electrostatic association of a porphyrin and CNDs on ammonium functionalized MoS₂ and WS₂,^{17, 18} should be mentioned. Markedly, femtosecond transient absorption studies on covalently modified TMDs revealed that upon photoexcitation of CNDs and TMDs ultrafast energy transfer from excited CNDs to MoS₂ and WS₂ occurs, while when preferentially exciting the TMDs within the hybrid materials, charge transfer in CND-MoS₂ but not in CND-WS₂ was identified.¹⁶ Conversely, it was revealed that the characteristic photoluminescence of porphyrin was quenched by the presence of MoS₂ and WS₂ within the corresponding nanoensembles formed by electrostatic interactions, revealing transduction of energy from the photoexcited porphyrin, acting as electron donor, to MoS₂ or WS₂ acting as electron acceptors.¹⁷ Furthermore, the electrocatalytic activity of electrostatically bound CNDs/MoS₂ ensembles towards the hydrogen evolution reaction was assessed and attributed to enhanced charge-transfer kinetics owed to the intimate contact between the two species as well as the presence of active sites in MoS₂.¹⁸

On the other hand, polythiophenes, belonging to the greater family of conjugated polymers, exhibit environmentally stable behavior and can find useful applications in organic electronics such as for example in field effect transistors, organic solar cells and organic light emitting devices.¹⁹ However, a major drawback of unsubstituted polythiophenes is their poor solubility in organic solvents, which limits sufficient manipulation in wet conditions and handicaps processing and fabrication. Therefore, to overcome this hurdle, specific design of the reactive monomer unit, incorporating solubilizing side-chains, plays a crucial role for achieving

polythiophenes with sufficient solubility, that can ultimately facilitate thin-film handling. Furthermore, these side-chains offer opportunities for spontaneous self-assembling of the polymeric species, thus inducing formation of crystalline domains, which in turn improve the electronic and optical properties.²⁰ To this end, introducing a charged side chain to a polymer backbone brings aqueous solubility on the corresponding derivatives of polythiophene.²¹ Moreover, the presence of charged groups creates an environment for the development of donor-acceptor ensembles based on attractive electrostatic interactions, which may promote effective electron and/or energy transfer processes to happen between the components of the ensemble. Hence, aqueous polythiophenes became attractive and important materials for the development of environmentally friendly hybrid materials for optoelectronic devices.²² For instance, a water soluble polythiophene derivative was combined with graphene quantum dots to yield hybrid nanostructures, which upon fabrication in an organic photovoltaic device exhibited a power-conversion efficiency of 1.76%.²² Conversely, incorporating C₆₀ as electron acceptor species within water-soluble polythiophene micelles, resulted in quenching of the emission of polythiophene, indicating the development of photoinduced excited state interactions.²³

Based on the aforementioned considerations, it is absolutely timely to integrate a water-soluble polythiophene to TMDs and thoroughly examine the corresponding ensembles to gain insights into the optoelectronic properties. To achieve this, (a) polythiophene was specifically modified to bear carboxylic units, which can be easily ionized to the corresponding carboxylates, on its skeleton, and (b) exfoliated MoS₂ and WS₂ were chemically modified such as to carry ammonium units. Herein, we report on the electrostatic association of poly(3-thiophene sodium acetate) **1** with positively charged modified MoS₂ **2a** and WS₂ **2b**, yielding in a controlled fashion poly(3-thiophene sodium acetate)/MoS₂ and poly(3-thiophene sodium acetate)/WS₂

ensembles **3a** and **3b**, respectively. The newly formed **3a** and **3b** were characterized via complementary spectroscopic and electron microscopy imaging techniques and their optical/photophysical and photoelectrochemical properties were investigated. Since the redox potentials of poly(3-thiophene sodium acetate) **1** are properly aligned with the conduction band energy of MoS₂ and WS₂, photoinduced intra-ensemble charge-transfer processes were exploited and assessed by photoluminescence titrations assays. Specifically, strong quenching of the characteristic emission of poly(3-thiophene sodium acetate) **1** in the presence of modified MoS₂ and WS₂ within ensembles **3a** and **3b** was evident, showcasing the energetically favored photoexcited electron transfer from **1** to the conduction band of MoS₂ and WS₂. Alongside, the improvement of the photoanodic response for **3a** and enhancement of the photocurrent for **3b** further proved the development of strong interactions between the individual components of the ensembles. Overall, the current study not only provides perceptions to incorporate new functional species within TMDs furnishing hybrid materials with on-demand characteristics, but also highlights the significance of interfacing aqueous polythiophene with properly functionalized MoS₂ and WS₂ in solar-light harvesting and optoelectronic applications.

EXPERIMENTAL SECTION

Instrumentation. Steady-state UV-Vis electronic absorption spectra were recorded on a PerkinElmer (Lambda 19) UV-Vis-NIR spectrophotometer. Steady-state emission spectra were recorded on a Fluorolog-3 JobinYvon-Spex spectrofluorometer (model GL3-21). Picosecond time-resolved fluorescence spectra were measured by the time-correlated-single-photon-counting (TCSPC) method on a Nano-Log spectrofluorometer (Horiba Jobin Yvon), by using a laser diode as an excitation source (NanoLED, 375 nm) and a UV-Vis detector TBX-PMT series (250-850

nm) by Horiba Jobin Yvon. Lifetimes were evaluated with the DAS6 Fluorescence-Decay Analysis Software. Mid-infrared spectra in the region 500–4500 cm^{-1} were obtained on a Fourier transform IR spectrometer (Equinox 55 from Bruker Optics) equipped with a single reflection diamond ATR accessory (DuraSamp1IR II by SensIR Technologies). A drop of the solution was placed on the diamond surface, followed by evaporation of the solvent, in a stream of nitrogen, before recording the spectrum. Typically, 100 scans were acquired at 2 cm^{-1} resolution. Micro-Raman scattering measurements were performed at room temperature in the backscattering geometry using a RENISHAW inVia Raman microscope equipped with a CCD camera and a Leica microscope. A 2400 lines/mm grating was used for all measurements, providing a spectral resolution of $\pm 1 \text{ cm}^{-1}$. As an excitation source the Ar^+ laser (633 nm with less than 2.65 mW laser power) was used. Measurements were taken with 15 seconds of exposure times at varying numbers of accumulations. The laser spot was focused on the sample surface using a long working distance 50x objective. Raman spectra were collected on numerous spots on the sample and recorded with Peltier cooled CCD camera. The data were collected and analyzed with Renishaw Wire and Origin software. Thermogravimetric analysis was performed using a TGA Q500 V20.2 Build 27 instrument by TA in a nitrogen (purity >99.999%) inert atmosphere. Scanning electron microscope (SEM) imaging and energy dispersive X-ray spectroscopy (EDS) were performed using a FE-SEM (model JSM-7610F) equipped with an EDAX (X-ACT, Oxford instrument). Zeta potential studies were carried out using a Zeta-sizer NanoZS (Malvern instruments Ltd, UK). The electrochemical experiments were performed with a AUTOLAB PGSTAT302N potentiostat. Cyclic voltammetry assays were carried out in a three-electrode cell employing a 0.1 M NaClO_4 in dry acetonitrile as supporting electrolyte at a scan rate of 20 mV/s. Photoelectrochemical measurements were carried out on spray-coated samples on FTO

substrates (covering area 1 cm²) as working electrode, which were illuminated through a quartz window by a 150 W Xenon arc lamp (LOT-Oriel GmbH, Germany).

Synthesis of 3-thiophene methyl acetate. Thiophene-3-acetic acid (1 g) in dry methanol (20 mL) with a 0.05 mL H₂SO₄ was refluxed for 24 hours. Then, the reaction poured onto the ultrapure water and extracted with dichloromethane. The organic phase was dried over magnesium sulfate and the solvent was evaporated to furnish a pale-yellow liquid in 80 % yield.

Synthesis of poly(3-thiophene methyl acetate). The monomer 3-thiophene methyl acetate (2 mmol) was dissolved in dry chloroform (10 mL) and then FeCl₃ (8 mmol) dissolved in 10 mL of chloroform was added dropwise under an inert atmosphere. The reaction mixture was stirred at room temperature for 24 hours, then poured into methanol and the precipitate was filtered. The filtered polymer was washed with methanol and water several times to remove unreacted monomer and any FeCl₃ residue. The obtained poly (3-thiophene methyl acetate) was dried at room temperature overnight.

Synthesis of poly(3-thiophene sodium acetate) 1. Poly(3-thiophene methyl acetate) (100 mg), deionized water (50 mL) and aqueous 2 M NaOH (10 mL) were placed in a double-neck flask and refluxed overnight. After that period, the reaction mixture was filtered and the supernatant centrifuged at 4000 rpm for 5 minutes in order to remove any insoluble materials. The collected supernatant was transferred inside a dialysis tubing and dialyzed against deionized water for 3 days at room temperature. Subsequent evaporation of water by freeze-drying technique gave **1** as a reddish solid.

Preparation of 2a and 2b. Briefly, 50 mg of exfoliated semiconducting MoS₂ or WS₂ was added to 20 mg of the 1,2-dithiolane derivative carrying a *tert*-butyl carbamate (BOC) ethylene glycol side chain in 10 mL of DMF. The mixture was stirred at 70 °C for 3 days. After that

period, the reaction mixture was filtered through a PTFE membrane (0.2 μm pore size) and the solid residue was washed with dichloromethane. In order to cleave the BOC protecting group, 30 mg of the BOC-modified TMD-based materials were redispersed in dichloromethane and treated with gaseous HCl. The reaction mixture was left under stirring for 12 hours and then filtered through a PTFE membrane (0.2 μm pore size) to yield **2a** and **2b**.

Titration assays – preparation of 3a and 3b. Aliquots of aqueous **2a** or **2b** (0.33 mg/mL) were added to aqueous 1 (2 mL, 10 mM) and changes after each addition in the UV-Vis absorption and fluorescence emission spectra upon excitation at 395 nm were recorded.

RESULTS AND DISCUSSION

Based on the general functionalization methodology of exfoliated TMDs with 1,2-dithiolanes,¹⁵ treatment of exfoliated MoS₂ and WS₂ with the 1,2-dithiolane *tert*-butyl carbamate derivative shown in Figure 1, yielded the butoxycarbonyl (BOC)-modified MoS₂ and WS₂ materials. Acidic deprotection of the BOC group furnished the ammonium functionalized materials **2a** and **2b** (Figure 1). At this stage, two points should be noted (i) the presence of the solubilizing chain as addend on the modified MoS₂ and WS₂, in **2a** and **2b**, contributing to solubilization and allowing handling and characterization in liquid media, and (ii) the existence of positive charges, due to the incorporated ammonium species in **2a** and **2b**, which can be exploited in attractive electrostatic interactions. The structure of **2a** and **2b** was unambiguously proved and justified by IR and Raman spectroscopy, thermogravimetry (TGA), Kaiser test and ζ -potential assays. Without going into deep detail, (a) IR spectroscopy verified the success for the preparation of BOC-modified MoS₂ and WS₂ and the corresponding ammonium functionalized materials **2a** and **2b**, by observing spectral changes in the characteristic carbonyl vibrations due

to the amide and BOC moieties. Specifically, the BOC carbonyl stretching vibration located at 1710 cm^{-1} for the BOC-modified MoS_2 and WS_2 was missing in the spectra of the corresponding ammonium functionalized materials **2a** and **2b**, in which only the carbonyl amide at 1665 cm^{-1} was evident (Supporting Information, Figure S1), (b) Raman spectroscopy, performed under on-resonance conditions (633 nm for MoS_2 -based materials and 514 nm for WS_2 -based materials), proved the effective functionalization by revealing suppression of the 2LA(M) band, related to sulfur vacancies, at 460 and 350 cm^{-1} for **2a** and **2b** respectively, as compared to the one due to exfoliated MoS_2 and WS_2 (Supporting Information, Figure S2), respectively, (c) TGA allowed the estimation of one ammonium moiety for every 48 and 35 units of MoS_2 and WS_2 , respectively, by calculating the corresponding mass loss observed in the temperature range 250 - $540\text{ }^\circ\text{C}$ to be 2.6 and 2.3% for **2a** and **2b** (Supporting Information, Figure S3), respectively, while ζ -potential measurements revealed that the values obtained for exfoliated MoS_2 (-25.7 mV) and WS_2 (-31.5 mV) were significantly shifted to more positive values for **2a** (10.6 mV) and **2b** (6.9 mV) respectively, due to the presence of the positively charged ammonium moieties.

The synthesis of the poly(3-thiophene sodium acetate) **1** was accomplished via oxidative polymerization of 3-thiophene methyl acetate in the presence of iron(III) chloride.²⁴ Briefly, 3-thiophene acetic acid was initially esterified to the corresponding methyl acetate derivative, in order to protect the oxidative decomposition of the carboxylic acid side chain of the monomer during the oxidative coupling polymerization reaction.²⁵ Next, the thiophene ester was polymerized, by employing iron(III) chloride as oxidative coupling agent. Subsequent alkaline hydrolysis of the ester, resulted on the negatively charged water-soluble poly(3-thiophene sodium acetate) **1**, which was further purified by dialysis and obtained in powder form by

repetitive freeze-drying cycles. The structure of **1** was spectroscopically justified by FTIR and ^1H NMR (Supporting Information, Figures S4 and S5).

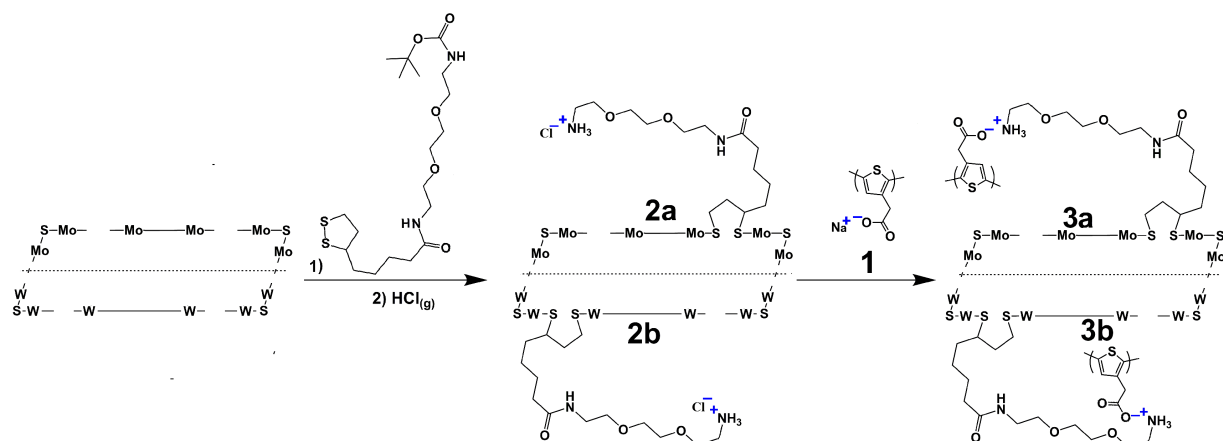


Figure 1. Illustrative preparation of ammonium functionalized MoS₂ **2a** and WS₂ **2b** and their electrostatic association with poly(3-thiophene sodium acetate) **1**, furnishing ensembles **3a** and **3b**, respectively.

The realization of ensembles **3a** and **3b** was accomplished upon addition of aqueous **2a** and **2b** to water-soluble **1**, by performing a series of titration assays, monitored with the aid of electronic absorption spectroscopy. In more detail, the UV-Vis spectrum of **1** exhibits a strong and broad absorption band around 400 nm due to π - π^* transitions of the conjugated polymer backbone, corresponding to the non-aggregated amorphous polymer domains.²⁴ Upon incremental additions of **2a** and **2b**, the excitonic bands of MoS₂ at 629 and 687 nm and of WS₂ at 654 nm started to evolve (Supporting Information, Figure S6). Please note that additional bands of MoS₂ due to indirect excitons at 481 and 523 and for WS₂ at 426, 481 and 566 nm (Supporting Information, Figure S7) were masked by the broad absorption of **1** in the visible region. Subtraction of the absorption background due to MoS₂ and WS₂ allowed a clear observation of the titration effect

on the polymer's absorption features, during formation of **3a** and **3b**. Specifically, a blue-shift of 4 and 9 nm of the polymer's band after a total of 290 μL and 40 μL was observed for **3a** and **3b**, respectively (Figure 2a and b). This hypsochromic shift corresponds to conformational changes on the structure of **1**, as the long π - π conjugation system of the coplanar polythiophene breaks²⁵ due to the developed attractive electrostatic interactions with the modified TMDs **2a** and **2b**. In addition, the absorption band due to **1** was progressively decreased upon interaction with **2a** and **2b**. Considering that the unstacked carboxylate unit absorbs more light in intact polymer **1**, the latter decrease identified in the corresponding absorption band of the ensembles **3a** and **3b** can be safely attributed to efficient interactions developed between the carboxylate units of **1** and the ammonium species of **2a** and **2b**, respectively. On the other hand, in blank titration assays performed by employing exfoliated MoS_2 and WS_2 instead of the positively charged **2a** and **2b**, neither a blue-shift nor a decrease in the polymer's absorption features were observed (Figure 2c and d), showcasing the role of modified MoS_2 and WS_2 with ammonium units for the effective Coulombic association with negatively charged **1**.

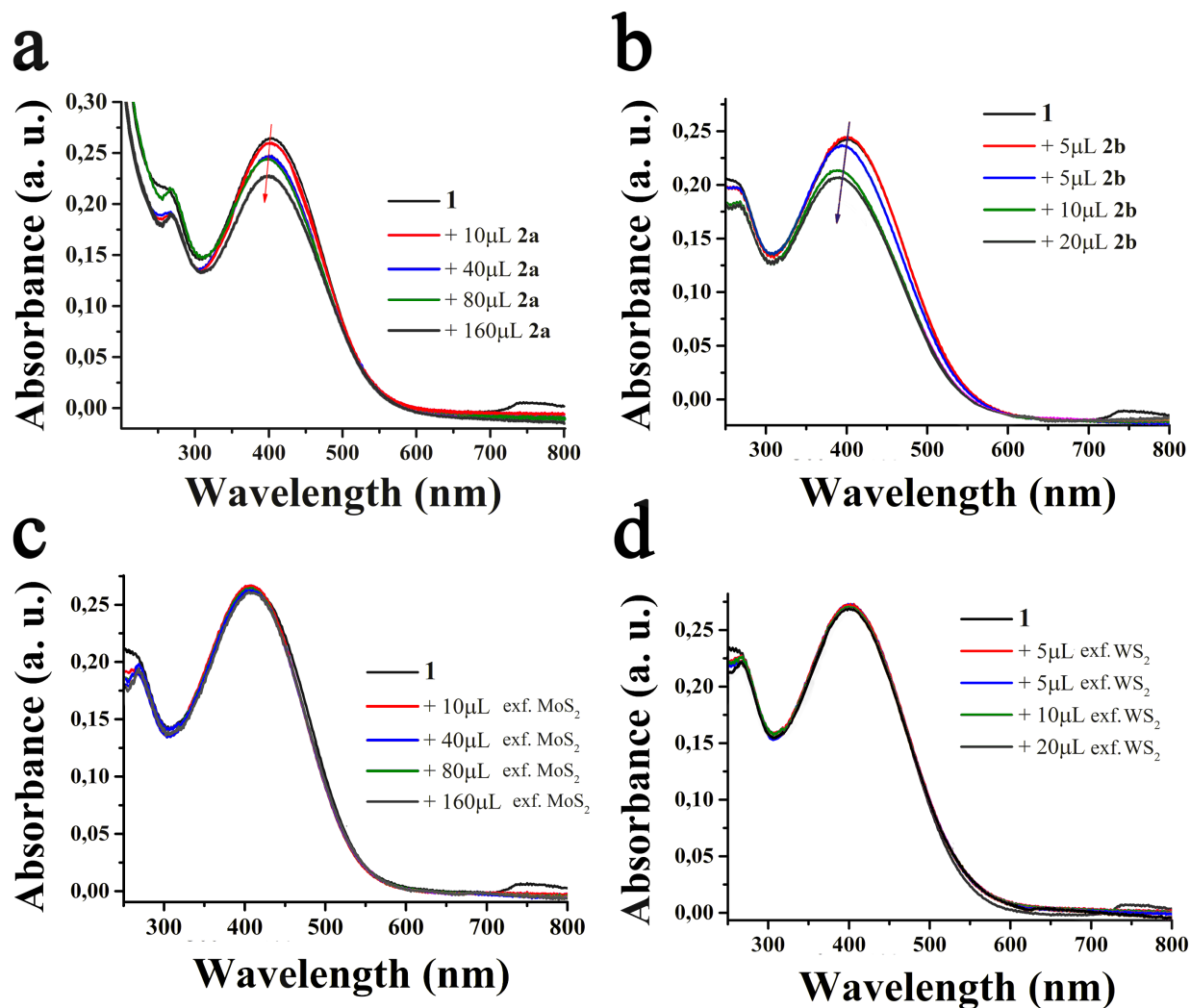


Figure 2. Electronic absorption spectra of **1** upon incremental additions of (a) ammonium functionalized material **2a**, forming ensemble **3a**, (b) ammonium functionalized material **2b** forming ensemble **3b**. UV-Vis blank titration assays of **1** upon incremental additions of exfoliated (c) MoS₂, and (d) WS₂.

Photoluminescence spectroscopy measurements were carried out to elucidate possible interactions at the excited states between **1** with **2a** and **2b**. Aqueous **1** exhibits fluorescence emission centered at 555 nm, upon excitation at 395 nm. This photoluminescence band gradually

decreases with increasing amounts of ammonium modified MoS₂ **2a** or WS₂ **2b** (Figure 3a and b), thereby leading to the realization of **3a** and **3b**, respectively. These outcomes prove the effective deactivation of the singlet excited state of **1** to MoS₂ and WS₂, via energy and/or electron transfer as the decay mechanism. Besides, when blank assays were investigated, by incorporating exfoliated MoS₂ and WS₂ instead of the positively charged ones, a substantially lower quenching rate for the emission of **1** was observed (Figure 3c and d). The observation of intra-ensemble photoinduced processes from poly(3-thiophene sodium acetate) **1** to MoS₂ and WS₂ is consistent with the oxidation potential of the former, precisely the energy of the singlet excited state of **1**, that lays above the conduction band of MoS₂ and WS₂. The energy for the singlet excited state of **1** can be easily obtained from the crossing point of the corresponding absorption and emission spectra (Supporting Information, Figure S8) and found to be 2.50 eV. On the other hand, the conduction band edges for MoS₂ and WS₂ were calculated to be 4.27 and 3.96 eV below the vacuum level, respectively, as a result of the higher reactivity of Mo vs W.²⁶ Hence, photoexcited electron/energy transfer from **1** to both MoS₂ and WS₂ within **3a** and **3b** respectively, is an energetically favored process. Moreover, the degree of fluorescence emission quenching of **1** in the presence of WS₂ is more prominent than that registered by MoS₂. For instance, for the quantitative emission quenching of **1** (2 mL, 10 mM) addition of 290 μ L of **2a** (0.33 mg/mL) is required, while only 40 μ L of **2b** (0.33 mg/mL) produces similar result – see Figure 3a and b. This fact is attributed to the smaller energy difference between the singlet excited state of **1** and the conduction band of WS₂, calculated to be 1.46 eV, as compared to that of MoS₂ which is calculated to be 1.77 eV.

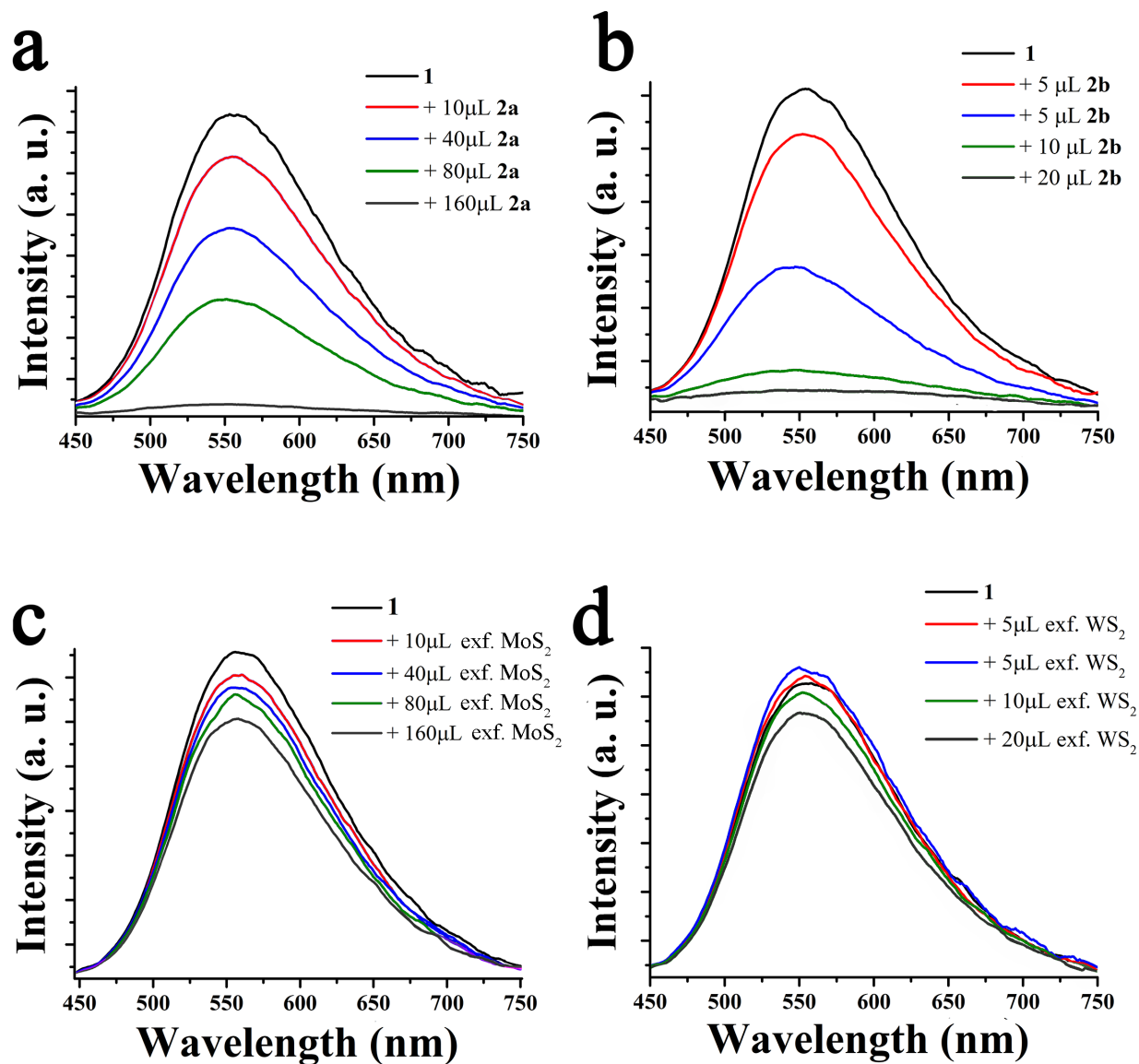


Figure 3. Photoluminescence spectra of **1** upon incremental additions of (a) ammonium modified MoS₂ **2a**, forming ensemble **3a**, (b) ammonium modified WS₂ **2b**, forming ensemble **3b**. Blank photoluminescence titration assays of **1** upon incremental additions of (c) exfoliated MoS₂, and (d) exfoliated WS₂. All measurements were conducted upon excitation at 395 nm.

In order to get additional insight on the electronic communication between **1** with MoS₂ and WS₂, within ensembles **3a** and **3b**, time-resolved photoluminescence assays based on the time-

correlated-single-photon-counting method were conducted. Polymer **1** shows a decay at 555 nm, which was monoexponentially fitted with a lifetime of 0.6 ns. On the other hand, **3a** and **3b** were better correlated with a biexponential fitting, which after analysis gave rise to lifetimes of 0.12 and 0.6 ns for **3a** and 0.14 and 0.6 ns for **3b**. While the slow lifetimes were identical to those due to free polymer **1**, the faster new ones 0.12 and 0.14 ns, for **3a** and **3b**, respectively, correspond to the fluorescence quenching of the emission intensity of the singlet excited state of the polymer within the ensembles **3a** and **3b**. Then, the quenching rate constant and quenching quantum yield were estimated for both **3a** and **3b** and presented in Table 1.

To further investigate the interactions between **1** with modified MoS₂ and WS₂ within ensembles **3a** and **3b**, Raman measurements were carried out under on-resonance conditions (633 nm for MoS₂-based materials and 514 nm for WS₂-based materials) on drop-casted films of the materials. Specifically, the Raman spectrum of MoS₂ is governed by four distinctive modes, namely, the 2LA(M) band located at 460 cm⁻¹ which is associated with sulfur defected sites, the A_{1g} band located at 406 cm⁻¹ which is associated with out-of-plane vibrations, the E_{2g} band located at 380 cm⁻¹ which is associated with in-plane vibrations and the two phonon difference combination mode of A_{1g}(M)-LA(M) located at 176 cm⁻¹ which is related to the asymmetry of few layered MoS₂. Markedly, the ammonium modified MoS₂ material **2a** was characterized by alterations in intensity of the 2LA(M) mode as compared with that due to exfoliated MoS₂. The intensity ratio $I_{2LA(M)}/I_{A1g}$ was decreased to 0.85 for **2a**, from the value of 2.09 due to exfoliated MoS₂ (Supporting Information, Figure S2), in agreement with earlier reports.^{13,27} The decrease in the intensity of the 2LA(M) band for the functionalized materials **2a** comes as result of the reduced number of sulfur defects due to edge functionalization of MoS₂. As far as ensemble **3a** concerns, on top of the aforementioned observations, an additional band at 1460 cm⁻¹ after

subtracting the intense fluorescence of **1**, was observed (Figure 4a). The latter band is due to the C=C of the thiophene ring²⁸ and found to be red-shifted by 5 cm⁻¹ as compared with the corresponding band registered for intact **1**. Similar is the situation with the Raman spectra due to WS₂-based materials. In this case, WS₂ shows Raman features at 350, 355 and 419 cm⁻¹, related with the 2LA(M), E¹_{2g} and A_{1g} modes, respectively. Again, the 2LA(M) band was found decreased for the modified material **2b** as compared to that belonging to exfoliated WS₂, while in ensemble **3b** the band due to the C=C of the thiophene was red-shifted by 10 cm⁻¹ centered at 1455 cm⁻¹ as compared to intact **1**.

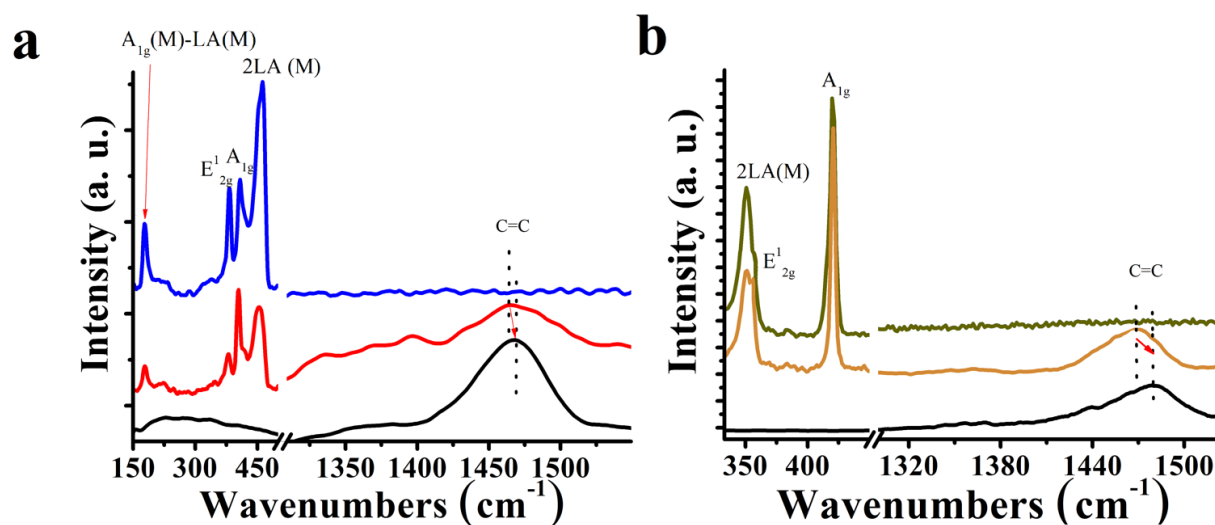


Figure 4. Raman spectra for (a) exfoliated MoS₂ (blue), ensemble **3a** (red), **1** (black), obtained upon 633 nm excitation, and (b) exfoliated WS₂ (olive), ensemble **3b** (brown) and **1** (black), obtained upon 514 nm excitation

The morphology of modified TMDs **2a** and **2b** was paralleled with that of ensembles **3a** and **3b** and assessed by SEM imaging. Briefly, a few drops of aqueous dispersions of the materials were deposited by drop-casting onto the SEM sample holder and imaged after the solvent was slowly evaporated. From extensive imaging of several different areas and flakes, oligolayered

flat nanostructures lacking amorphous impurities with size of few hundred nanometers for **2a** and **2b** were evident (Figure 5a and b). It should be noted that the imaging of oligolayered flakes in **2a** and **2b** most likely derived from the restacking of TMD sheets as occurred during the drying process after being deposited on the SEM sample holder. In addition, the robust and continuous network shown in those images suggests the integrity of the basal plane in **2a** and **2b**, in other words free of defects basal plane, assuring the presence of high-quality materials with intact electronic properties, in accordance with the performed 1,2-dithiolane-based functionalization at the edge of the MoS₂ and WS₂ layers. Similar images were acquired for **3a** and **3b** (Figure 5c and d), though it can be clearly seen that MoS₂ and WS₂ were covered by soft organic matter due to the presence of polymer **1**. The latter is further corroborated by the lack of crystallinity as the commonly observed flat structures of TMDs appeared wrinkled and roughen upon integration of **1**.

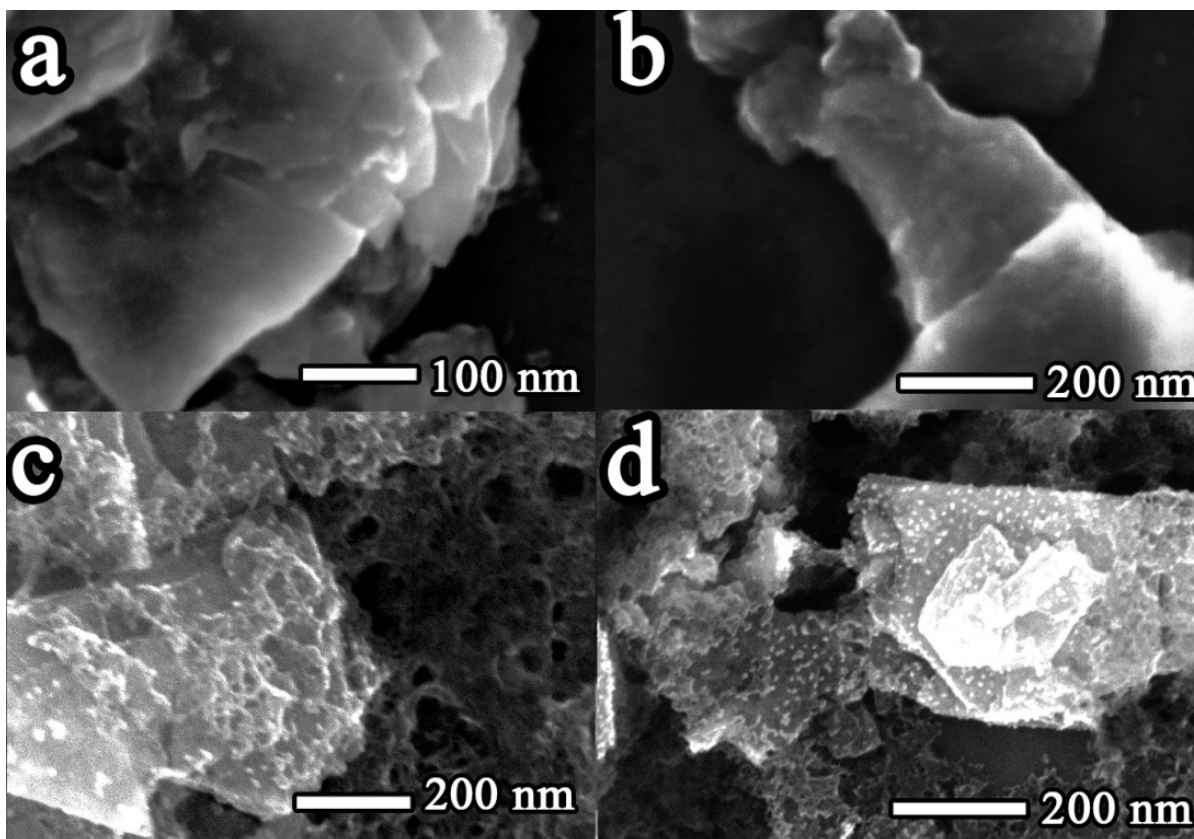


Figure 5. Representative FE-SEM images for (a) **2a**, (b) **2b**, (c) **3a** and (d) **3b**.

The electronic interactions identified between the two components in ensembles **3a** and **3b** were further examined by photoelectrochemical measurements. Precisely, dark cyclic voltammetry (CV) assays of **1** showed a voltammogram qualitatively similar to analogous polythiophene derivatives.²⁹ Specifically, the CV of **1** (Supporting Information, Figure S9) was governed by a capacitive behavior at potentials below 0.6 V, and displayed a faradaic feature beyond this value, corresponding to the regions of the bandgap and valence band of **1**, respectively. On the other hand, exfoliated WS₂ and MoS₂ dark voltammograms showed a typical capacitive behavior, with no remarkable redox features. The background current for MoS₂ was lower than that for WS₂, which suggests a lower electrochemical active area and/or lower conductivity of the material.³⁰ Focusing on ensembles **3a** and **3b**, some key differences were observed under dark current assays. In the case of **3a**, the CV showed an enhancement of the current at negative potential values, indicative of strong interactions between MoS₂ and **1** at the level of MoS₂ conduction band. By contrast, **3b** exhibited a CV similar to that of free polymer **1** (Supporting Information, Figure S9), however, with a higher value for the electrochemical capacitive current in the bandgap region due to the presence of WS₂. Next, CV under on-off illumination conditions for **1** revealed a photocathodic response (Figure 6a), typical of p-doped materials. The cathodic photocurrent started at ca. 0.8 V and reached a maximum value of -1.1 $\mu\text{A}/\text{cm}^2$, while a small anodic photocurrent, reaching 0.1 $\mu\text{A}/\text{cm}^2$, appeared in positive scans, at potentials higher than 0.8 V (Figure 6b). For exfoliated MoS₂ and WS₂, both photocathodic and photoanodic currents were observed. Notably, for exfoliated WS₂, the photocathodic current (-0.33 $\mu\text{A}/\text{cm}^2$ at 0.21 V) was higher than the photoanodic one (0.14

$\mu\text{A}/\text{cm}^2$ at 0.12 V). For exfoliated MoS_2 the opposite phenomenon was observed and the photocathodic response was very low ($-0.02 \mu\text{A}/\text{cm}^2$ at 0.07 V), while the photoanodic current was rather high ($0.09 \mu\text{A}/\text{cm}^2$ at 0.46 V), though still lower than that registered for exfoliated WS_2 . The photopotential and photocurrent values for WS_2 thus reveal favorable transfer of both electrons and holes to the solution underlining its ability to act as p- and n-doped material. For MoS_2 , however, mostly holes are transferred to the solution, thus performing as an n-doped material in these conditions.

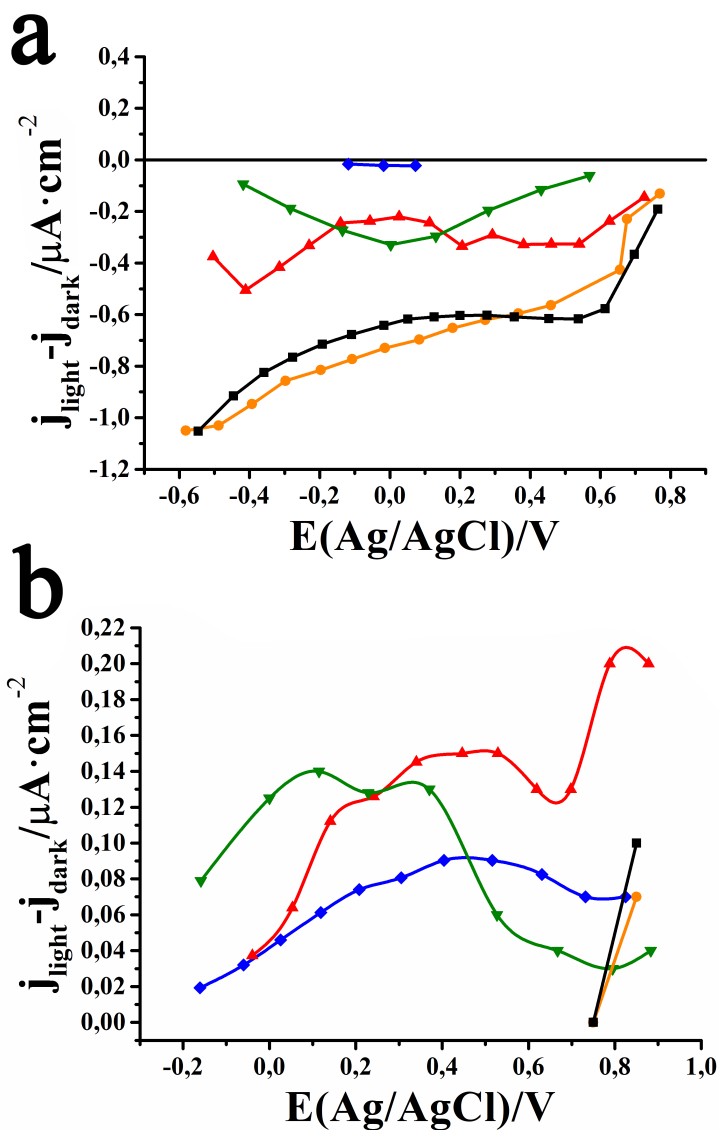


Figure 6. Photocurrents obtained by on-off cyclic voltammetry (a) photocathodic branch, and (b) photoanodic branch, for **1** (black), **3a** (red), **3b** (orange), exfoliated MoS₂ (blue) and exfoliated WS₂ (olive), obtained at a scan rate of 20 mV/sec and with 0.1 M NaClO₄ as electrolyte.

The behavior of **3b** was qualitatively similar to that of **1**, with a very similar but smaller photoanodic response in the positive scan ($0.07 \mu\text{A}/\text{cm}^2$ at 0.85 V). In the negative scan, however, there was observed a decrease of the photocurrent at potentials higher than 0.3 V, with a difference of $0.13 \mu\text{A}/\text{cm}^2$ at 0.6 V, and an increase in the photocurrent value at potentials lower than 0.3 V, with a difference of $0.09 \mu\text{A}/\text{cm}^2$ at -0.1 V. The latter finding shows the existence of charge-transfer phenomena between **1** and WS₂, within ensemble **3b**. Particularly, WS₂ accepts photoelectrons from **1** and transfers them to the solution, while increasing cathodic photocurrent at low potentials. At potentials higher than 0.3 V, the current decreased due to the activity of generated photoholes, which start to react with the species present in the solution, resulting in an overall decrease of the net cathodic photocurrent. In contrast, MoS₂ was not electrochemically active towards photoreduction. Therefore, photoelectron transfer from MoS₂ in **3a** yielded a clear decrease in the photocathodic current ($-0.24 \mu\text{A}/\text{cm}^2$ at 0.60 V), since the photoelectrons were not easily transferred to the solution. Furthermore, photoanodic current was clearly observed, opposite to the case for **3b**, and even enhanced with respect to exfoliated MoS₂ (with two peaks, giving $0.15 \mu\text{A}/\text{cm}^2$ at 0.5 V and $0.20 \mu\text{A}/\text{cm}^2$ at 0.84 V). Here, the availability of photoholes for the oxidation was not masked by the presence of active photoelectrons for photoreduction. A collection of the photoelectrochemical and photophysical parameters for ensembles **3a** and **3b** is shown in Table 1.

Table 1. Summary of photoelectrochemical and photophysical data for ensembles **3a** and **3b** as well as poly(3-thiophene sodium acetate) **1** and exfoliated MoS₂ and WS₂.

Materials	Anodic photocurrent <i>j</i> (μA/cm ²)	Cathodic photocurrent <i>j</i> (mA/cm ²)	τ _f (ns) ^a	k _q ^s (s ⁻¹) ^b	Φ _q ^s ^c
1	0.1 (at 0.85 V)	-0.60 (at 0.60 V) -0.68 (at -0.10 V)	0.6		
3a	0.15 (at 0.50 V) 0.2 (at 0.84 V)	-0.26 (at 0.60 V) -0.24 (at -0.40 V)	0.12 / 0.6	6.67x10 ⁹	0.80
3b	0.07 (at 0.85 V)	-0.47(at 0.60 V) -0.77 (at -0.10 V)	0.14 / 0.6	5.48x10 ⁹	0.78
Exfoliated MoS₂	0.09 (at 0.46 V)	-0.02 (at 0.07 V)			
Exfoliated WS₂	0.14 (at 0.12 V)	-0.31 (at 0.02 V)			

^a λ_(exc) = 376 nm; λ_(em) = 555 nm

^b The quenching rate constant k_q^s is derived by the equation: k_q^s = 1/τ_f - 1/τ₀

^c The quenching quantum yield Φ_q^s is derived by the equation: Φ_q^s = (1/τ_f - 1/τ₀)/(1/τ_f)

In the above equations, τ₀ is the lifetime of free polymer **1** and τ₀ is the lifetime of polymer in the corresponding ensemble **3a** and **3b**.

Finally, the observation of both positive and negative photocurrent intensities at the same applied potential for WS₂, MoS₂ and **3a**, as a function of the scan direction, suggests an

important inertness of the photoinduced charges to follow the applied electric field causing a photoinduced memory effect. While this explains concomitantly competing photoanodic and photocathodic contributions in our measurement, this effect, moreover, is reminiscent of a photomemristor behavior,³¹ thus opening new pathways for forthcoming studies on TMD-based materials.

CONCLUSION

The integration of poly(3-thiophene sodium acetate) **1** with ammonium functionalized MoS₂ and WS₂ materials **2a** and **2b**, forming novel aqueous and stable donor-acceptor nanoensembles **3a** and **3b**, respectively, was accomplished. The presence of side chains featuring carboxylate anions in the polythiophene backbone of **1** was beneficial for the development of attractive electrostatic interactions with the positively charged ammonium moieties, covalently grafted via the 1,2-dithiolanes functionalization route, on modified MoS₂ and WS₂ materials **2a** and **2b**, respectively. Electronic absorption and fluorescence emission titration assays proved the creation of ensembles **3a** and **3b**. Notably, progressive quenching of the characteristic emission of **1** at 555 nm upon incremental additions of **2a** and **2b** suggested the existence of energy and/or electron transfer as channel for the deactivation of the singlet excited state of **1** to MoS₂ and WS₂. Photoelectrochemical assays confirmed the existence of intra-ensemble electronic interactions and revealed the establishment of photo-induced charge-transfer processes. Here, **3a** exhibited an enhanced photoanodic current offering additional channels for hole-transfer to the solution, while **3b** displayed an increased photocathodic current providing supplementary pathways of electron-transfer to the solution. Moreover, the observed inertness of the photoinduced charges to follow the applied electric field upon reversal of the scan direction not

only facilitates concomitantly competing photoanodic and photocathodic processes contributing to the distinct photoresponse behavior of **3a** and **3b**, but even more reveals the existence of unique photoinduced memory effects in these novel donor-acceptor materials. All in all, the outcome of the current study showcases the significance of TMD-based donor-acceptor ensembles in optoelectronics and photoelectrochemical applications, while it is expected to further encourage and motivate additional explorations of diverse TMD-based ensembles and their performance in charge-transfer processes.

ASSOCIATED CONTENT

Supporting Information

ATR-IR, Raman, NMR, UV-Vis and fluorescence emission spectra, TGA graphs and cyclic voltammograms. The Supporting Information is available free of charge on the ACS Publications website.

AUTHOR INFORMATION

Corresponding Author

* Nikos Tagmatarchis, E-mail: tagmatar@eie.gr

* Ana M. Benito, E-mail: abenito@icb.csic.es

* Wolfgang K. Maser, E-mail: wmaser@icb.csic.es

Author Contributions

These authors have equally contributed.

ACKNOWLEDGMENT

This project has received funding from the European Union's Horizon 2020 research and innovation programme under the Marie Skłodowska-Curie grant agreement N° 642742. Support of this work by the projects "Advanced Materials and Devices" (MIS 5002409) which is implemented under the "Action for the Strategic Development on the Research and Technological Sector", and "National Infrastructure in Nanotechnology, Advanced Materials and Micro- / Nanoelectronics" (MIS 5002772) which is implemented under the "Reinforcement of the Research and Innovation Infrastructures", funded by the Operational Program "Competitiveness, Entrepreneurship and Innovation" (NSRF 2014-2020) and co-financed by Greece and the European Union (European Regional Development Fund) to N. T. is acknowledged. A.M.B. and W.K.M further acknowledge Spanish *MINEICO* (project grant ENE2016-79282-C5-1-R), the *Gobierno de Aragón* (Grupo Reconocidos DGA-T03_17R), and associated EU Social Funds.

REFERENCES

1. Wang, Q. H.; Kalantar-Zadeh, K.; Kis, A.; Coleman, J. N.; Strano, M. S. Electronics and Optoelectronics of Two-Dimensional Transition Metal Dichalcogenides. *Nat. Nanotechnol.* **2012**, *7*, 699-712.
2. Lee, K.; Gatensby, R.; McEvoy, N.; Hallam, T.; Duesberg, G. S. High-Performance Sensors Based on Molybdenum Disulfide Thin Films. *Adv. Mater.* **2013**, *25*, 6699-6702.

3. Pospischil, A.; Furchi, M. M. & Mueller, T. Solar-Energy Conversion and Light Emission in an Atomic Monolayer p–n Diode. *Nat. Nanotechnol.* **2014** *9*, 257-261.
4. Stephenson, T.; Li, Z.; Olsen, B.; Mitlin, D. Lithium Ion Battery Applications of Molybdenum Disulfide (MoS₂) Nanocomposites. *Energy Environ. Sci.* **2014**, *7*, 209-231.
5. Xu, M.; Liang, T.; Shi, M.; Chen, H. Graphene-Like Two-Dimensional *Materials*. *Chem. Rev.* **2013**, *113*, 3766-3798.
6. Rowley-Neale, S.; Foster, C.; Smith, G.; Brownson, D.; Banks, C. E. Mass-Produced, 2D-MoSe₂ Bulk Modified Screen-Printed Electrodes Provide Significant Electrocatalytic Performances Towards the Hydrogen Evolution Reaction. *Sustainable Energy Fuels* **2017**, *1*, 74-83.
7. Perivoliotis, D. K.; Tagmatarchis, N. Recent Advancements in Metal-Based Hybrid Electrocatalysts Supported on Graphene and Related 2D Materials for the Oxygen Reduction Reaction. *Carbon* **2017**, *118*, 493-510.
8. Bertolazzi, S.; Gobbi, M.; Zhao, Y.; Backes, C.; Samori, P. Molecular Chemistry Approaches for Tuning the Properties of Two-Dimensional Transition Metal Dichalcogenides. *Chem. Soc. Rev.* **2018**, *47*, 6845-6888.
9. Ryder, C. R.; Wood, J. D.; Wells, S. A.; Hershman, M. C. Chemically Tailoring Semiconducting Two-Dimensional Transition Metal Dichalcogenides and Black Phosphorus. *ACS Nano* **2016**, *10*, 3900-3917.

10. Mak, K. F.; Lee, C.; Hone, J.; Shan, J.; Heinz, T. F. Atomically Thin MoS₂: A New Direct-Gap Semiconductor. *Phys. Rev. Lett.* **2010**, *105*, 136805.
11. Zhao, W.; Ghorannevis, Z.; Chu, L.; Toh, M.; Kloc, C.; Tan, P. -H.; Eda, G. Evolution of Electronic Structure in Atomically Thin Sheets of WS₂ and WSe₂. *ACS Nano* **2013**, *7*, 791-797
12. Voiry, D.; Goswami, A.; Kappera, R.; Silva, C. d. C. C.; Kaplan, D.; Fujita, T.; Chen, M.; Asefa, T.; Chhowalla, M. Covalent Functionalization of Monolayered Transition Dichalcogenides by Phase Engineering. *Nature Chem.* **2015**, *7*, 45-49.
13. Knirsch, K. C.; Berner, N. C.; Nerl, H. C.; Cucinotta, C. S.; Gholamvand, Z.; McEvoy, N.; Wang, Z.; Abramovic, I.; Vecera, P.; Halik, M.; Sanvito, S.; Duesberg, G. S.; Nicolosi, V.; Hauke, F.; Hirsch, A.; Coleman, J. N.; Backes, C. Basal-Plane Functionalization of Chemically Exfoliated Molybdenum Disulfide by Diazonium Salts. *ACS Nano* **2015**, *9*, 6018-6030.
14. Chen, X.; Berner, N. C.; Backes, C.; Duesberg, G. S.; McDonald, A. R. Functionalization of Two-Dimensional MoS₂: On the Reaction Between MoS₂ and Organic Thiols. *Angew. Chem. Int. Ed.* **2016**, *55*, 5803-5808.
15. Canton-Vitoria, R.; Sayed-Ahmad-Baraza, Y.; Pelaez-Fernandez, M.; Arenal, R.; Bittencourt, C.; Ewels, C. P.; Tagmatarchis, N. Functionalization of MoS₂ with 1,2-Dithiolanes: Toward Donor-Acceptor Nanohybrids for Energy Conversion. *NPJ 2D Mater. Appl.* **2017**, *1*, 13.

16. Vallan, L.; Canton-Vitoria, R.; Gobeze, H. B.; Jang, Y.; Arenal, R.; Benito, A. M.; Maser, W. K.; D'Souza, F.; Tagmatarchis, N. Interfacing Transition Metal Dichalcogenides With Carbon Dots for Managing Photoinduced Energy and Charge-Transfer Processes", *J. Am. Chem. Soc.* **2018**, DOI: 10.1021/jacs.8b09204.
17. Canton-Vitoria, R.; Stangel, C.; Tagmatarchis, N. Electrostatic Association of Ammonium-Functionalized Layered-Transition-Metal Dichalcogenides with an Anionic Porphyrin. *ACS Appl. Mater. Interfaces* **2018**, *10*, 23476-23480.
18. Canton-Vitoria, R.; Vallan, L.; Urriolabeitia, E.; Benito, A. M.; Maser, W. K.; Tagmatarchis, N. Electronic Interactions in Illuminated Carbon Dot/MoS₂ Ensembles and Electrocatalytic Activity Towards Hydrogen Evolution. *Chem. Eur. J.* **2018**, *10*, 10468-104674.
19. Skotheim T. A.; Reynolds, J. R.; eds., Handbook of Conducting Polymers; CRC Press: Boca Raton, FL, 2007, Chapter 9, pp. 1-39.
20. Sheina, E. E.; Sonya M.; Khersonsky, Jones, E. G.; McCullough, R. D. Highly Conductive, Regioregular Alkoxy-Functionalized Polythiophenes: A New Class of Stable, Low Band Gap Materials. *Chem. Mater.* **2005**, *17*, 3317-3319.
21. Zhu, C.; Liu, L.; Yang, Q.; Lv, F.; Wang, S.; Water-Soluble Conjugated Polymers for Imaging, Diagnosis, and Therapy. *Chem. Rev.* **2012**, *112*, 4687-4735.
22. Routh, P.; Das, S.; Shit, A.; Bairi, P.; Das, P.; Nandi, A. K.; Graphene Quantum Dots from a Facile Sono-Fenton Reaction and Its Hybrid With a Polythiophene Graft

- Copolymer Toward Photovoltaic Application. *ACS Appl. Mater. Interfaces* **2013**, *5*, 12672-12680.
23. Cheng, C.-C.; Lin W.-L.; Liao, Z.-S.; Chu, C.-W.; Huang, J.-J.; Huang, S.-Y.; Fan W.-L.; Lee, D.-J.; Water-Soluble Fullerene-Functionalized Polymer Micelles for Efficient Aqueous-Processed Conductive Devices. *Polym. Chem.* **2017**, *8*, 7469-7474.
24. Istif, E.; Hernández-Ferrer, J.; Urriolabeitia, E. P.; Stergiou, A.; Fratta, G.; Tagmatarchis, N.; Large, M. J.; Dalton, A. B.; Benito, A. M.; Maser, W. K. Conjugated Polymer Nanoparticles – Graphene Oxide Charge-Transfer Complexes. *Adv. Funct. Mater.* **2018**, *28*, 1707548.
25. Kim, B.-S.; Chen, L.; Gong, J.; Osada, Y. Titration Behavior and Spectral Transitions of Water-Soluble Polythiophene Carboxylic Acids. *Macromolecules* **1999**, *32*, 3964-3969.
26. Gong, C.; Zhang, H.; Wang, W.; Colombo, L.; Wallace, R. M.; Cho, K. Band Alignment of Two-Dimensional Transition Metal Dichalcogenides: Application in Tunnel Field Effect Transistors. *Appl. Phys. Lett.* **2013**, *103*, 053513.
27. Benson, E. E.; Zhang, H.; Schuman, S. A.; Nanayakkara, S. U.; Bronstein, N. D.; Ferrere, S.; Blackburn, J. L.; Miller, E. M. Balancing the Hydrogen Evolution Reaction, Surface Energetics, and Stability of Metallic MoS₂ Nanosheets via Covalent Functionalization. *J. Am. Chem. Soc.* **2018**, *140*, 441-450.
28. Tsoi, W. C.; James, D. T.; Kim, J. S.; Nicholson, P. G.; Murphy, C. E.; Bradley, D. D. C.; Nelson, J.; Kim, J.-S. The Nature of In-Plane Skeleton Raman Modes of P3HT and

their Correlation to the Degree of Molecular Order in P3HT:PCBM Blend Thin Films. *J. Am. Chem. Soc.* **2011**, *133*, 9834-9843.

29. Braunger, M. L.; Barros, A.; Ferreira, M.; Olivati, C. A. Electrical and Electrochemical Measurements in Nanostructured Films of Polythiophene Derivatives. *Electrochim. Acta* **2015**, *165*, 1-6.

30. Fabregat-Santiago, F.; Mora-Seró, I.; Garcia-Belmonte, G.; Bisquert, J. Cyclic Voltammetry Studies of Nanoporous Semiconductors. Capacitive and Reactive Properties of Nanocrystalline TiO₂ Electrodes in Aqueous Electrolyte. *J. Phys. Chem. B* **2003**, *107*, 758-768.

31. Wang, W.; Panin, G. N.; Fu, X; Zhang, L.; Ilanchezhian, P.; Pelenovich, V.O.; Fu, D.; Kang, W.T. MoS₂ Memristor With Photoresistive Switching. *Sci. Rep.* **2016**, *6*, 31224.